J. Min. Metall. Sect. B-Metall. 60 (1) (2024) 59 - 70

Journal of Mining and Metallurgy, Section B: Metallurgy

STUDY ON THE BEHAVIOR OF IMPURITY REMOVAL FROM LITHIUM-IRON-PHOSPHATE SLAG USING THE ULTRASONIC-ASSISTED SULPHURIC ACID LEACHING

Y. Zhao [a], Y.-H. Wang [a], J.-J. Wu [a, b], W.-H. Ma [a, b]

[a] Faculty of Metallurgical and Energy Engineering, Kunming University of Science and Technology, Kunming, People's Republic of China

[b] National Engineering Research Center of Vacuum Metallurgy, Kunming University of Science and Technology, Kunming, People's Republic of China

(Received 10 August 2023; Accepted 02 February 2024)

Abstract

The recovery of iron phosphate from the leaching slag of used lithium iron phosphate cathode materials is a crucial step to achieve closed-loop recovery of lithium iron phosphate, which has not yet been effectively accomplished. In the study, ultrasonic-assisted sulfuric acid leaching was used to remove impurities in the iron phosphate, to meet the stringent impurity content requirements for battery-grade iron phosphate regarding impurity content. Optimization of leaching conditions involved a sulfuric acid concentration of 0.2 mol·L^{-1}, acid-leaching time of 30 min, power of 50 W, and reaction temperature of 80℃. Under these conditions, the removal efficiencies of Cr, Cu, Ni, and Zn in iron phosphate were 26.09%, 83.0%, 75.9%, and 96.3%, respectively. Simultaneously, the content of impurity elements Cr and Zn concurred with the standard for battery-grade iron phosphate (HG/T 4701-2021), with both 50 ppm and 10 ppm contents. The leaching results indicated the effectiveness of ultrasound in enhancing the removal of impurity elements in iron phosphate within a sulfuric acid solution. Further analyses, including XRD, particle size, TEM, and XPS indicated that the surface of the iron phosphate particles cavitated after ultrasonic acid leaching, resulting in the formation of numerous pores. Additionally, particle collisions led to a reduction in particle size, with no generation of by-products during the process. This innovative approach not only contributed to the removal of impurity elements but also provided insights into the reuse of leaching slag (iron phosphate) and offered guidance for the recovery of metals from waste lithium iron phosphate cathode materials.

Keywords: *Iron phosphate; Ultrasonic acid leaching; Battery-grade; Reuse*

1. Introduction

The lithium, iron, and phosphorus resources inherent in discarded lithium iron phosphate cathode materials represent valuable metallic assets [1, 2]. The recycling of these materials not only yields economic value but also serves to reduce environmental pollution [3, 4]. A leach solution, enriched with metal ions was derived from waste lithium iron phosphate cathode materials using hydrometallurgical method [5]. The controlled precipitation of metal ions under specific conditions resulted in the formation of metal products, facilitating metal recovery [6, 7]. However, this method of recycling metal from waste lithium iron phosphate cathode materials inevitably generates leaching slag, a residue comprising residual iron and phosphorus after the recovery of lithium [8, 9]. Improper handling of this residual slag poses a risk of wasting valuable metal resources and causing environmental pollution, emphasizing the imperative need for recycling [10, 11]. Studies have shown that the physical phase of leaching slag is primarily iron phosphate, making the regeneration of battery-grade iron phosphate crucial for the closed-loop recovery of lithium iron phosphate [12, 13]. Interestingly, this vital aspect has been overlooked and remains unrealized. Iron phosphate derived from leaching slag, holds potential as a raw material for manufacturing lithium iron phosphate cathode materials [13]. To harness the reuse of iron phosphate in the leaching slag, stringent control of impurity elements within iron phosphate is essential to meet purity requirements for raw material [14].

Given this objective, this study focused on the removal of impurity elements, namely Cr, Cu, Ni, and Zn, from iron phosphate, proposing an innovative "waste into wealth", guiding the efficient and environmentally friendly recycling of waste lithium

Corresponding author: dragon_wu213@126.com

https://doi.org/10.2298/JMMB230810005Z

iron phosphate cathode materials [15]. This study introduced ultrasonic enhancement technology to remove impurity elements, promoting a closed-loop recycling process for the utilization of lithium iron phosphate cathode materials. The experiments employed ultrasonic-assisted sulfuric acid conditions, exploring the effects of time, power, and reaction temperature on impurity removal. The optimal conditions for impurity removal were determined, accompanied by an in-depth analysis of the underlying mechanism.

2. Experiments

2.1. Experimental materials

The chemicals used, including sulfuric acid (98 wt% H_2SO_4) and hydrogen peroxide (30 wt% H_2O_2), were of analytical grade and used without purification. The experimental material consisted of leaching slag produced during the leaching process of waste lithium iron phosphate cathode material. In Fig. 1(a), XRD analysis confirmed the physical phase of the leaching slag as iron phosphate (PDF#34-0134). As a raw material for lithium-ion batteries cathode preparation, iron phosphate must meet strict requirements for impurity elements Cr, Cu, Ni, and Zn. ICP-OES analysis revealed that the content of these elements in the iron phosphate exceeded the specified limits (Table 1).

From Table 1, it was observed that the iron phosphate as a raw material for the preparation of cathode materials for lithium-ion batteries met industry requirements for Cr ≤ 50 ppm, Cu ≤ 8 ppm, Ni ≤ 20 ppm, and Zn ≤ 50 ppm. The ICP-OES analysis results indicated that the content of Cr, Cu, Ni, and Zn in the iron phosphate was 69 ppm, 1000 ppm, 830 ppm, and 27 ppm. The particle size analysis of iron phosphate was conducted and the results are shown in Fig. 1(b). The particle size analysis of iron phosphate indicated a particle size distribution with D10 = 4.66 μm, D50 = 9.45 μm, D90 = 14.95 μm, and D99 = 19.68 μm. These values elucidated the size distribution of iron phosphate particles, essentially assessing its suitability as a raw material for cathode materials.

2.2. Experimental process

Water was introduced to fill two-thirds of the ultrasonic cleaner volume, followed by preheating the water to match the temperature specified in the experimental design. Subsequently, 1.6 g of the iron phosphate was weighed and introduced into a pre-prepared sulfuric acid solution of known concentration (the leaching solution was 100 mL). The addition of hydrogen peroxide solution was a gradual process. The beaker was then sealed and positioned within the ultrasonic cleaner for heating. The power of the ultrasonic cleaner was systematically adjusted to align with the experimental design conditions. Upon completion of the acid-leaching experiment, both the heating and ultrasonic power controls of the ultrasonic cleaner were deactivated. Subsequently, the beaker was promptly

Table 1. *Content of impurity elements in iron phosphate*

Element	Cr	Cu	Ni	Zn
Raw material (ppm)	69	1000	830	27
Lithium battery enterprises (ppm)	≤ 50	≤ 8	≤ 20	≤ 50

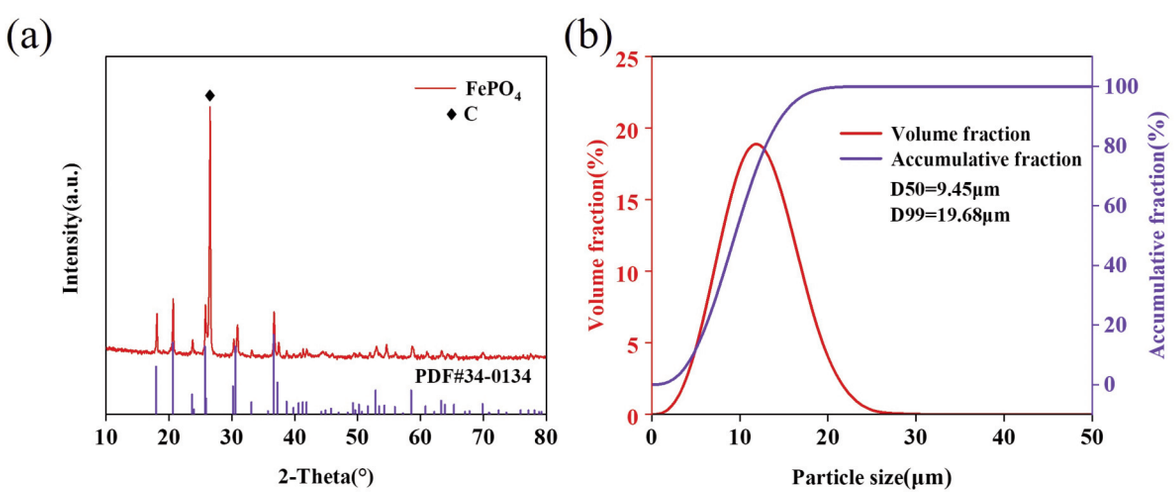

Figure 1. *(a) XRD analysis results of iron phosphate; (b) Particle size analysis of iron phosphate*

removed for filtration and separation. The leaching slag of the iron phosphate underwent multiple rinses during the filtration process. The filtered filter cake was dried in a vacuum drying oven for 12 h. After drying, the content of the impurity elements was analyzed through ICP-OES.

The removal efficiency of Cr, Cu, Ni, and Zn is expressed using Equation (1):

$$\tau = \frac{A - B}{A} \cdot 100\% \quad (1)$$

Where denotes the content of Cr, Cu, Ni, and Zn in the iron phosphate (ppm); denotes the content of Cr, Cu, Ni, and Zn in the iron phosphate after acid leaching (ppm); and denotes the removal efficiency of Cr, Cu, Ni, and Zn (%).

2.3. Removal principle

Under ultrasonic-assisted sulfuric acid conditions for removing impurity elements in iron phosphate, the underlying removal mechanism relies on ultrasound waves propagating through the liquid. This action induces liquid flow and the creation of numerous minuscule bubbles. These bubbles form and expand within negative pressure zones, swiftly collapsing within positive pressure zones—a phenomenon known as cavitation [16, 17]. Therefore, when the bubbles ruptured, it generated an impact force and a significant amount of energy. This resulted in an instantaneous high-pressure impact on the material, causing it to collide and fragment into smaller particles. This process significantly enhanced the surface area of the material available for reaction contact, thereby augmenting its dissolution in the acid [18]. This mechanism is illustrated in Fig. 2.

2.4. Characterization techniques

X-ray diffractometer (XRD, X'pert^{3}Powder, Netherlands) was employed to characterize the iron phosphate and iron phosphate leaching slag. ICP-OES (ICP-OES, 7700x, USA) was employed to analyze the content of the impurity elements in iron phosphate. The morphological changes of iron phosphate before and after ultrasonic leaching were analyzed using a high-resolution transmission electron microscope (TEM, TecnaiF20, USA, FEI Company). The particle size of the iron phosphate was analyzed using a laser particle size analyzer (Winner2000, Jinan, China). To clarify the change of chemical valence state of elements in the iron phosphate before and after ultrasonic leaching, X-ray photoelectron spectroscopy (XPS, PHI5000VersaProbe-Ⅱ, Japan) was used to conduct the analysis.

3. Results and discussion

3.1. Effect of sulfuric acid concentration on impurity removal

In elucidating the effectiveness of ultrasound in facilitating the removal of impurity elements in the acid-leaching process of iron phosphate, it is necessary to discuss the effect of the concentration of the acid-leaching solution on the removal of impurity elements. Hence, before conducting experiments to determine the optimized conditions for ultrasonic-assisted sulfuric acid removal of impurity elements

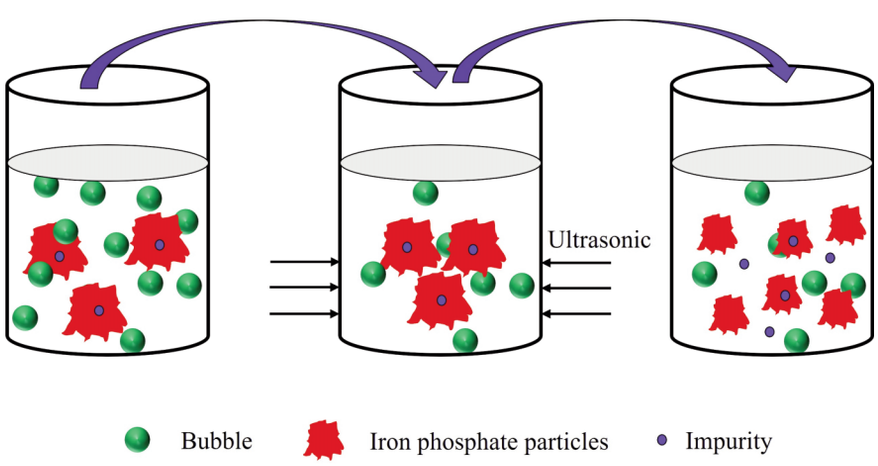

Figure 2. *Schematic diagram of ultrasonic acid leaching for removal of impurity elements from iron phosphate*

Table 2. *Conditions of leaching experiments*

Experiment	Sulfuric acid concentration	Power (W)	Time (h)	Reaction temperature (°C)
1	sulfuric acid	50	1	80
2	4 mol·L^{-1}	50	3	80

from iron phosphate, leaching experiments were conducted under different acid concentration conditions (Table 2).

To elucidate the leaching results of the iron phosphate under different acid concentration conditions, the leaching slag of the iron phosphate was subjected to XRD physical phase analysis. The XRD analysis results of the leaching slag of the iron phosphate under different acid concentrations were consistent (thus, this study presented a singular set of graphs), and the results are shown in Fig. 3.

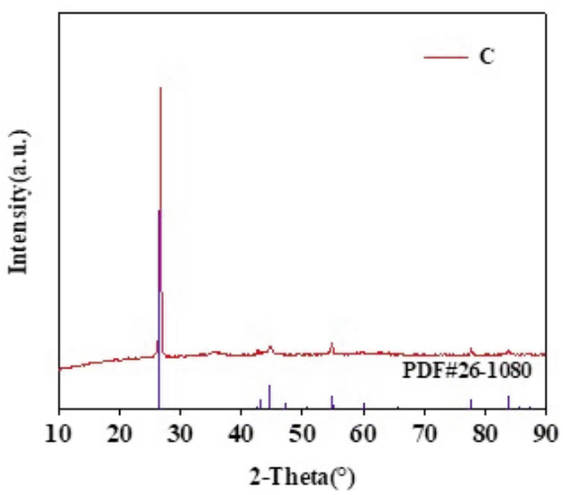

Figure 3. *XRD patterns of leaching of iron phosphate at different sulfuric acid concentrations*

The XRD analysis results from Fig. 3 indicated that the physical phase of the leached slag was C (graphite), which was derived from conductive carbon black and polyvinylidene fluoride binder for lithium iron phosphate batteries. Fig. 3 shows that dilute sulfuric acid (4 mol·L^{-1}) and concentrated sulfuric acid serving as leaching solution fragmented the structure of the iron phosphate, resulting in its complete dissolution into the solution in the form of ions. Therefore, to preserve the crystal structure of the iron phosphate, a low concentration of sulfuric acid served as the leaching solution. The combination of a low-concentration sulfuric acid solution and ultrasonic assistance was more advantageous in highlighting the enhanced efficacy of ultrasonic action in removing impurities such as Cr, Cu, Ni, and Zn from iron phosphate.

3.2. Effect of time on impurity removal

Based on the above experimental results, the experimental design conditions were sulfuric acid concentration of 0.2 mol·L^{-1}, power of 50 W, and reaction temperature of 80°C. Figs. 4(a) and (b) depict the analysis of the removal effect of the acid-leaching time on Cr, Cu, Ni, and Zn. Upon increasing the acid-leaching time from 20 min to 90 min, the contents of Cr, Cu, Ni, and Zn decreased, indicating that acid leaching exhibited a significant effect on the removal of impurity elements. When the acid-leaching time reached 20 min, the contents of Cr, Cu, Ni, and Zn were 50 ppm, 160 ppm, 210 ppm, and 10 ppm, and the removal rates were 27.54%, 84%, 74.7%, and 62.96%, respectively. Notably, the contents of Cr and Zn met industry requirements. Upon extending the acid-leaching time from 20 min to 50 min, the content of Cr, Cu, Ni, and Zn continued to decrease. Thus, the removal rates of Cr, Cu, Ni, and Zn were 34.78%, 86%, 77.11%, and 77.78%, respectively. However, with a further extension to 90 min, contents of Cr, Cu, Ni, and Zn increased slightly compared with that at 50 min, indicating a reduction in the removal effect of impurity elements with prolonged leaching time. Therefore, the leaching time was identified to be between 20 min and 50 min, with 30 min selected for subsequent experiments to conserve energy consumption.

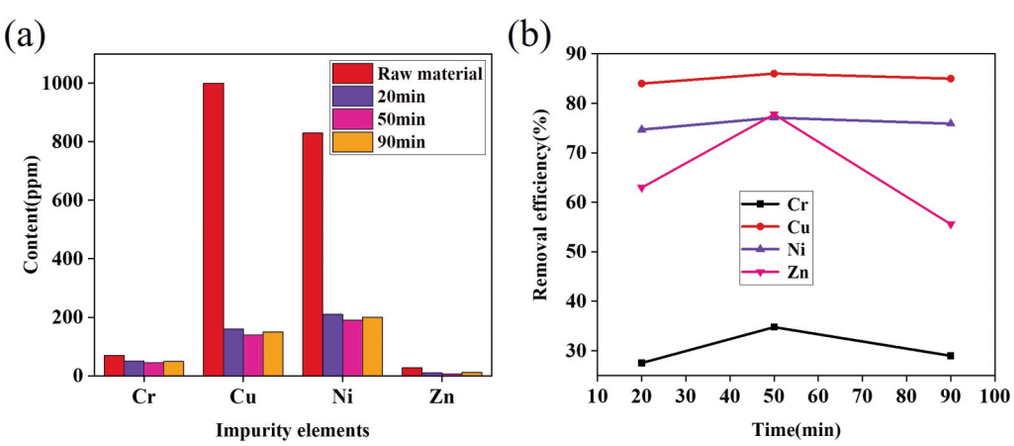

Figure 4. *Effect of acid leaching time on the removal of impurity elements*

3.3. Effect of power on impurity removal

Theoretically, stronger ultrasonic waves facilitate surface cavitation, forming voids and breaking particles into smaller fragments via collision. This process increased the contact reaction area of the particles and acid solution, ultimately enhancing the removal efficiency of impurity elements [19]. Under specific conditions (sulfuric acid concentration of 0.2 mol·L^{-1}, acid-leaching time of 30 min, and reaction temperature of 80°C), the removal effects of Cr, Cu, Ni, and Zn were studied under three different powers of 15 W, 35 W, and 50 W (Figs. 5(a) and (b)). From Fig. 5, it was observed that as power gradually increased, the contents of Cr, Cu, Ni, and Zn exhibited a gradual decreasing trend. When the power was 15 W, the contents of Cr, Cu, Ni, and Zn were 62 ppm, 190 ppm, 370 ppm, and 10 ppm, and the removal rates were 10.14%, 81%, 55.42%, and 62.96%, respectively. Furthermore, upon increasing the power to 35 W, the removal rate of Ni increased significantly. The Ni removal rate was 74.7%, while the Cr, Cu, and Zn removal rates were marginal. Subsequently, increasing the power to 50 W, the contents of Cr, Cu, Ni, and Zn exhibited a slight decrease. In comparing the 20 min in Fig. 4 with the 15 W influence factor experiment in Fig. 5, the results indicated that the power exhibited a significant influence on the removal of Cr, Cu, Ni, and Zn than that of the acid-leaching time. At 50 W, the contents of Cr and Zn met the requirements of the Chinese chemical industry standard for battery-grade iron phosphate (HG/T4701-2014), leading to the determination that 50 W was the optimal power for the experiment.

3.4. Effect of reaction temperature on impurity removal

The experiments were conducted in a low concentration of sulfuric acid solution, omitting the consideration of its effect on impurity element removal. The impact of reaction temperatures (35°C, 50°C, and 65°C, and the removal rate at 80°C is shown in Fig. 4) on impurity elements removal was studied under the conditions of sulfuric acid concentration of 0.2 mol·L^{-1}, power of 50 W, and acid-leaching time of 30 min (Figs. 6(a) and (b)). Fig. 6 illustrates that with an increased reaction temperature, the content of impurity Ni decreased, while Cr and Zn exhibited minimal changes. The content of Cu remained relatively stable, indicating that the reaction temperature exhibited less influence on the removal of impurity elements.

Upon optimizing the conditions affecting the removal of impurity elements, the optimal ultrasonic acid-leaching conditions were obtained as follows: sulfuric acid concentration of 0.2 mol·L^{-1}, acid-leaching time of 30 min, power of 50 W, and reaction temperature of 80°C. Under these conditions, the removal of Cr, Cu, Ni, and Zn from iron phosphate was achieved, with removal rates of 26.09%, 83.0%, 75.9%, and 96.3%, respectively. Impurity elements were effectively removed from iron phosphate via ultrasonic acid leaching. The existence of impurity elements can be explained by doping into the iron phosphate lattice, and impurities that cannot be removed by conventional acid leaching need to be removed by external forces that break the lattice and expose the impurity elements [20].

To study the leaching behavior of Cr, Cu, Ni, and Zn during acid leaching, the thermodynamic characteristics of the different metal phases, especially the stable regions, were analyzed using Eh-pH diagrams in HSC 6.0 software. Fig. 7(a) shows the Eh-pH diagram of the Cr-H_2O system, where the Cr (III) phase reached a redox potential of -0.4299 V–1.4756 V. It was acid-soluble in this stable region at a pH of 2.0768, providing an easily achievable leaching condition. The Eh-pH plot of the Zn-H_2O system in Fig. 7(d) expresses the same

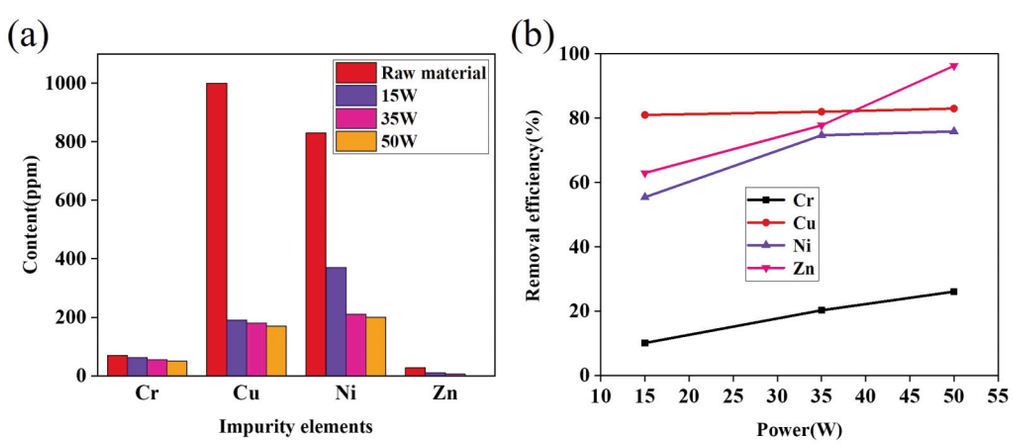

Figure 5. *Effect of power on the removal of impurity elements*

information. Specifically, the Zn (II) phase was soluble in acid at a redox potential of -0.7630V–2.0 V, and at a pH of 5.6077. Fig. 7(b) depicts the Eh-pH diagram of the Cu-H_2O system, indicating that the soluble Cu (II) phase was formed under strongly acidic and strongly reducing conditions. Fig. 7(c) depicts the Eh-pH diagram of the Ni-H_2O system, revealing that the Ni (II) phase was soluble in acid at a redox potential of -0.2367 V–2.0 V, and at a pH of 4.8912. The above analysis indicated that the leaching conditions for Cr and Zn were more conducive than those for Cu and Ni. This observation correlated with the findings of the study, indicating that the contents of Cr and Zn met the standard requirements after undergoing acid-leaching treatment. The use of ultrasonic-assisted leaching

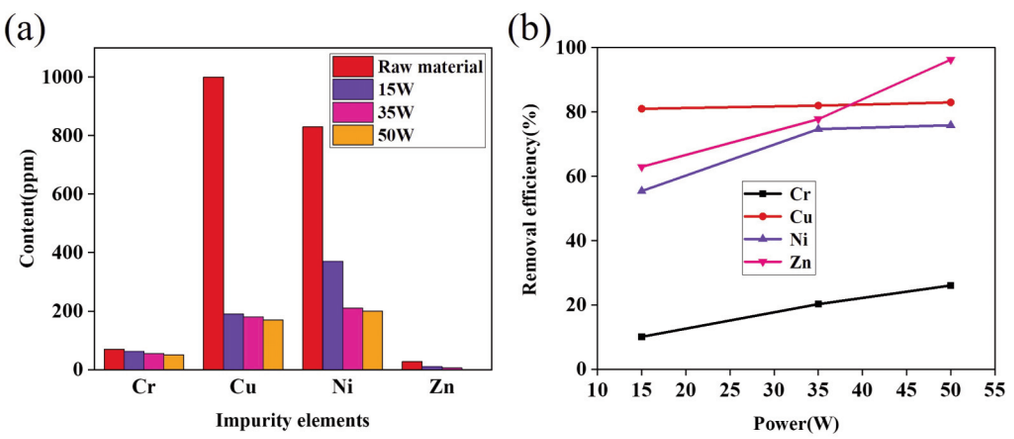

Figure 6. *Effect of reaction temperature on the removal of impurity elements*

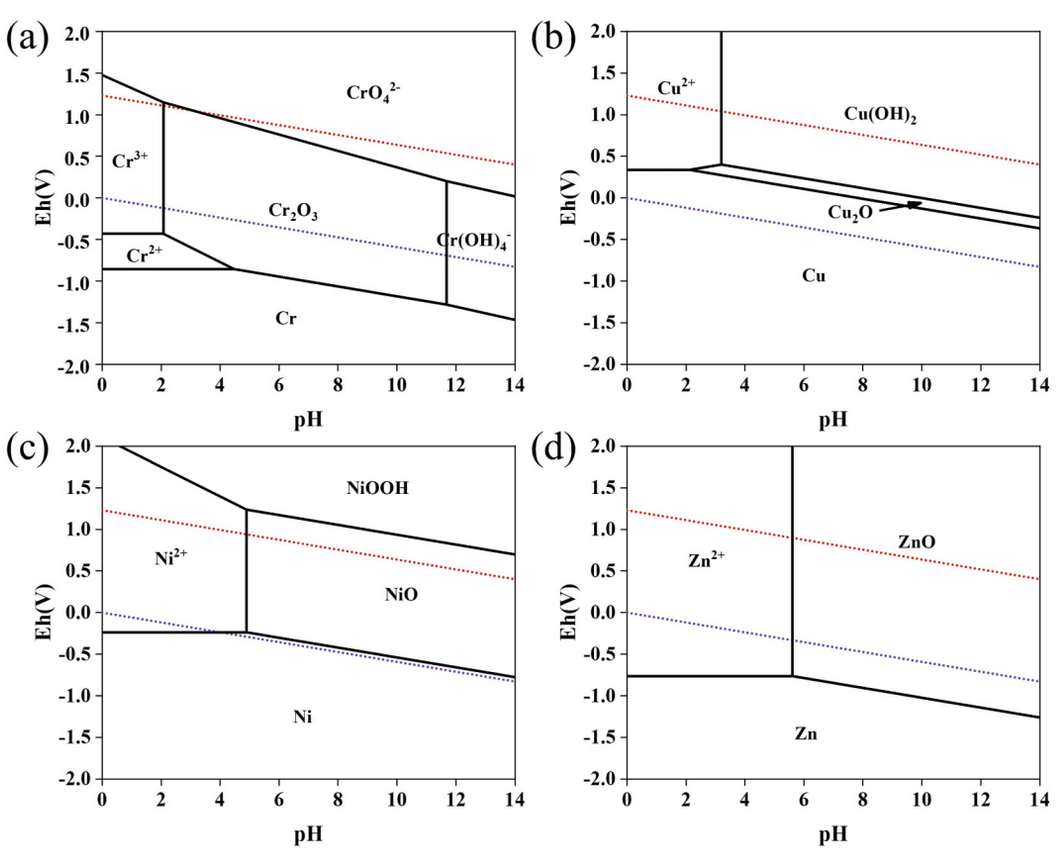

Figure 7. *Eh-pH diagram of Cr, Cu, Ni and Zn leaching system (concentration =1.0 M at 298 K and 1 atm pressure): (a) Cr-H_2O; (b) Cu-H_2O; (c) Ni-H_2O; (d) Zn-H_2O*

method can reduce the amount of acid used and increase the contact between the solution and the impurities, which is an effective method to improve the removal of impurities.

3.5. Impurity phase change and characterization in the acid-leaching process

(1) Changes in the physical phase of iron phosphate

To analyze the removal mechanism of impurity elements in the ultrasonic acidic leaching process, the analysis and characterization of iron phosphate after leaching process, the characterization of iron phosphate after leaching under different powers was conducted. XRD was employed to analyze the physical phase of iron phosphate under different power, determining whether the iron phosphate particles changed during the leaching process. The XRD physical phase analysis results of iron phosphate after leaching under different powers are shown in Fig. 8. Additionally, with increasing power, the intensity of the iron phosphate diffraction peaks decreased sequentially, and no other phases were found to be generated. Thus, it was observed that the sulfuric acid did not react with iron phosphate to generate other products during the acid-leaching process.

(2) Morphology and structure characterization of iron phosphate

The TEM characterization results of iron phosphate before and after ultrasonic acid leaching are shown in Figs. 9(a)–(f). As seen in Figs. 9(a)–(c),

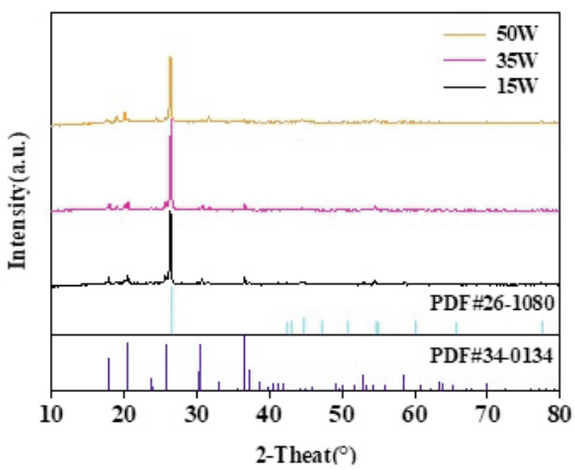

Figure 8. *Results of phase analysis of iron phosphate leaching under different power*

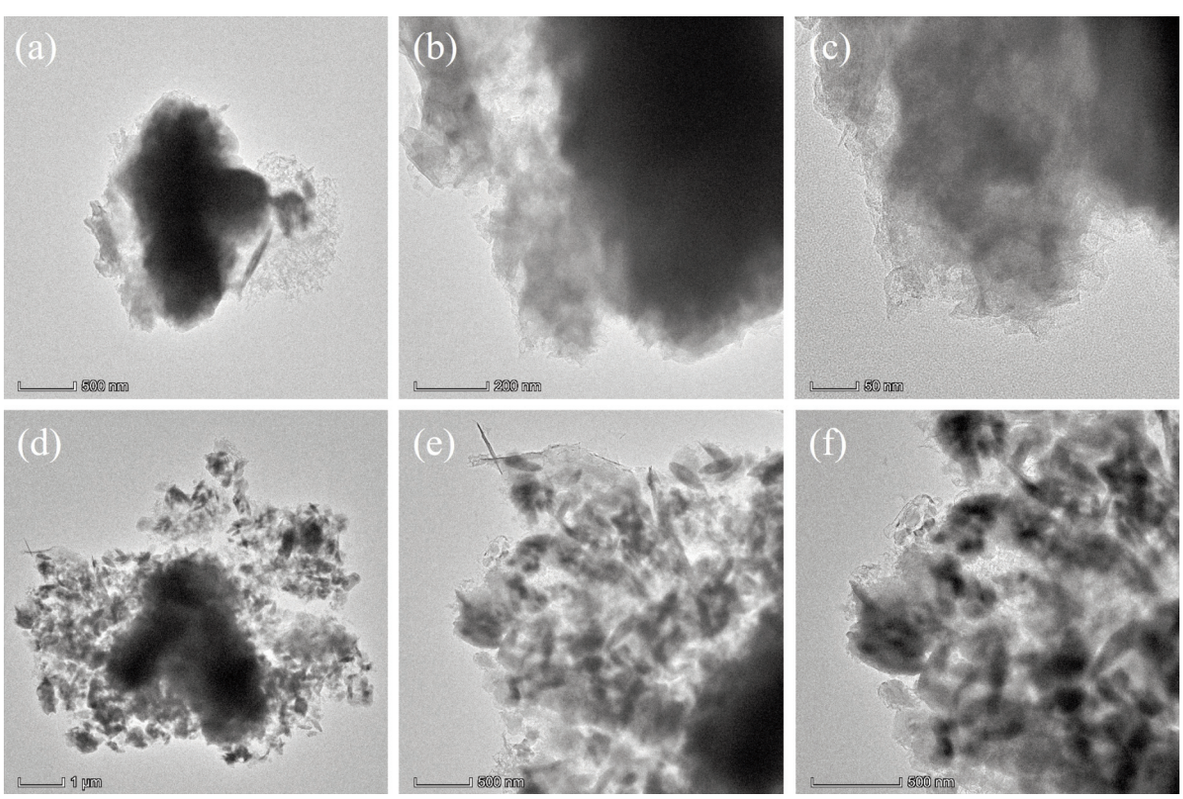

Figure 9. *Results of TEM characterization and analysis of iron phosphate: (a)-(c) without ultrasonic leaching of iron phosphate; (d)-(f) after ultrasonic leaching of iron phosphate*

the surface of iron phosphate particles before ultrasonic acid leaching was smooth and without notable cracks. From Figs. 9(d)–(f), it was seen that a large number of pores appeared on the surface of the iron phosphate after ultrasonic acid leaching, indicating that ultrasonic waves exhibited a cavitation effect on the particle surface. Furthermore, it was observed that the particle structure of iron phosphate particles was altered by ultrasonic energy [21, 22]. Therefore, after ultrasound treatment, the surface of the iron phosphate particles cavitated to form a large number of pores. This exposed the metal impurities and increased the reaction area to promote the chemical reaction between the impurities and the acid solution, facilitating the removal of impurity elements.

The results of XPS characterization analysis of the iron phosphate before and after ultrasonic acid leaching are shown in Figs. 10(a)–(h). The fine spectrograms of Fe2p in Figs. 10(a) and 10(e) exhibited two notable peaks at 725.9 eV and 712.2 eV, corresponding to $Fe2p_{1/2}$ and $Fe2p_{3/2}$ for Fe^{3+}, respectively [23, 24]. The fine spectrograms of P2p in Fig. 10(b) exhibited $P2p_{1/2}$ and $P2p_{3/2}$ at the binding energy located at 134.2 eV and the fine spectrograms of P2p in Fig.10(f) both corresponded to PO_4^{3-}. The C1s in Fig. 10(d) corresponded to C at the binding energy located at 284.5 eV, which correlated with the XRD analysis of the iron phosphate. However, the fine spectrogram of C1s in Fig. 10(h) exhibited a peak corresponding to Fe_3C at a binding energy of 283.9 eV, owing to the presence of Fe^{3+} in the solution. The XPS results indicated that the physical phase of the iron phosphate after ultrasonic acid leaching was $FePO_4$, corresponding to the results of the XRD analysis.

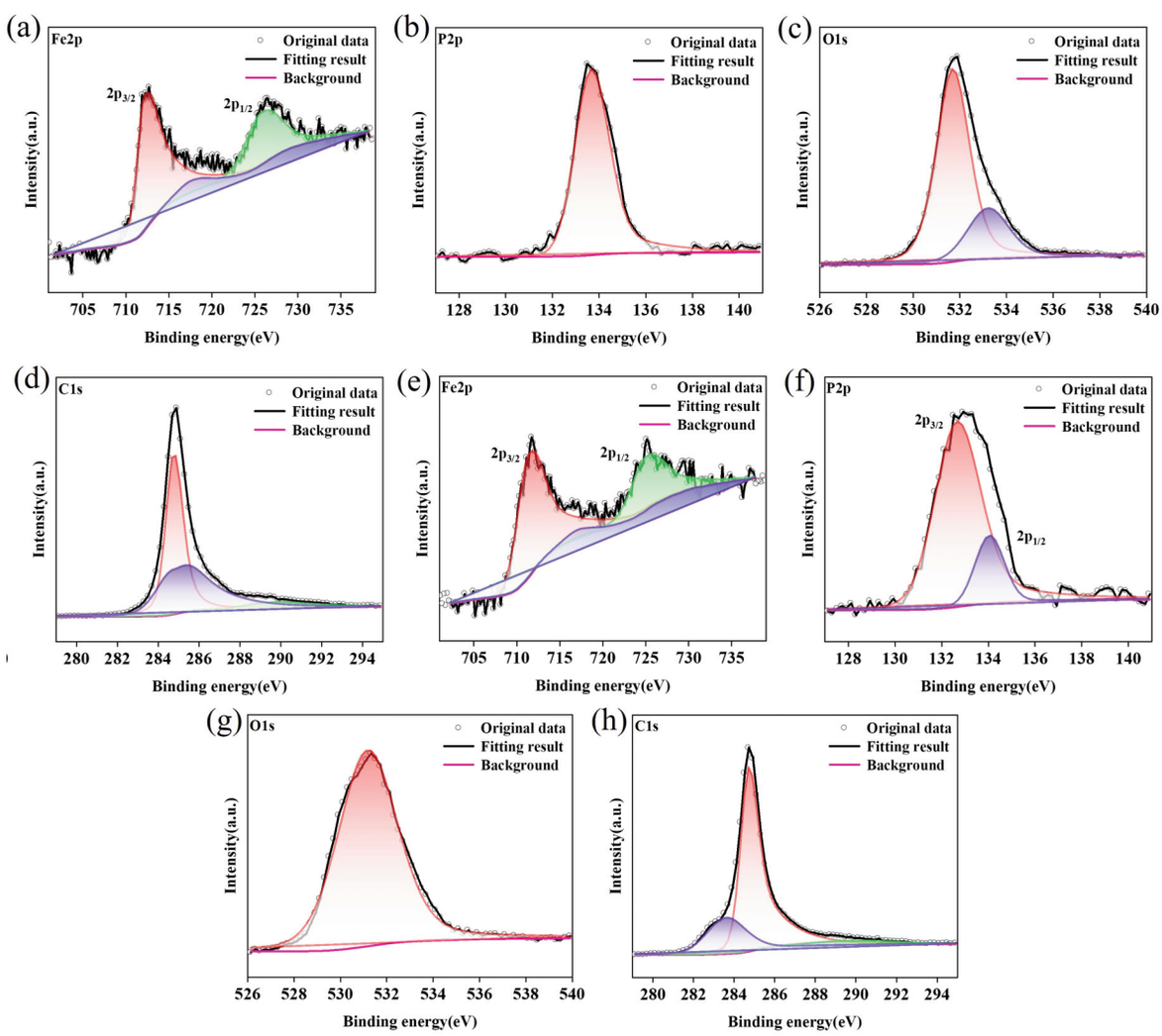

Figure 10. *Results of XPS characterization of iron phosphate: (a)-(d) without ultrasonic leaching of iron phosphate; (e)-(h) after ultrasonic leaching of iron phosphate*

3.6. Effect of ultrasound on particle size and morphology of iron phosphate

Particle size analysis and particle shape analysis of the iron phosphate at different powers were conducted (Fig. 11 and Table 3). It was observed from Fig. 11 that when the power was 15 W, the particle size distribution was D10 = 4.22 μm, D50 = 8.01 μm, D90 = 12.2 μm, and D99 = 15.34 μm. Similarly, at 35 W, the particle size distribution was D10 = 4.17 μm, D50 = 7.41 μm, D90 = 10.71 μm, and D99 = 13.61 μm. At 50 W, the particle size distribution was D10 = 4.14 μm, D50 = 7.22 μm, D90 = 10.33 μm, and D99 = 12.67 μm. Finally, when the power was 50 W, the particle size distribution was D10 = 4.14 μm, D50 = 7.22 μm, D90 = 10.33 μm, and D99 = 12.67 μm. It was evident that after ultrasonic acidic leaching, the particle size distribution interval was narrower, indicating that the particle distribution was more concentrated after leaching. As presented in Table 3, the standard deviation of D [3,2] and D [4,3] both decreased after ultrasonic acidic leaching, indicating that the particles of the iron phosphate were almost spherical after ultrasonic acidic leaching. Thus, the addition of ultrasonic destruction of the shape of the original iron phosphate resulted in more regular particles. Therefore, the removal process of metal impurities was accompanied by a change in the shape of the iron phosphate. Given the comprehensive analysis in Fig. 5, ultrasound fragmented the iron phosphate particles into tiny particles, increasing the contact area with the acid solution, and achieving the purpose of removing the impurity elements [24, 25]. Fig. 1 (b) and Fig. 11 illustrate a significant change in the particle size of the iron phosphate before and after ultrasonic leaching.

Additionally, when iron phosphate particles were leached in the acidic solution, voids formed on their surface under the action of ultrasound, leading to collisions, particle cracking, and size reduction. This process provided a gateway for the exposure and removal of impurity elements without generating other by-products.

Table 3. *Analysis results of shape parameters of iron phosphate particles under different power*
Note: D [3,2] - surface area average diameter and D [4,3] - volume average diameter

Particle size parameters	Iron phosphate	Power 15 W	Power 35 W	Power 50 W
D [3,2]	7.56	6.65	6.35	6.24
D [4,3]	9.64	8.10	7.43	7.23

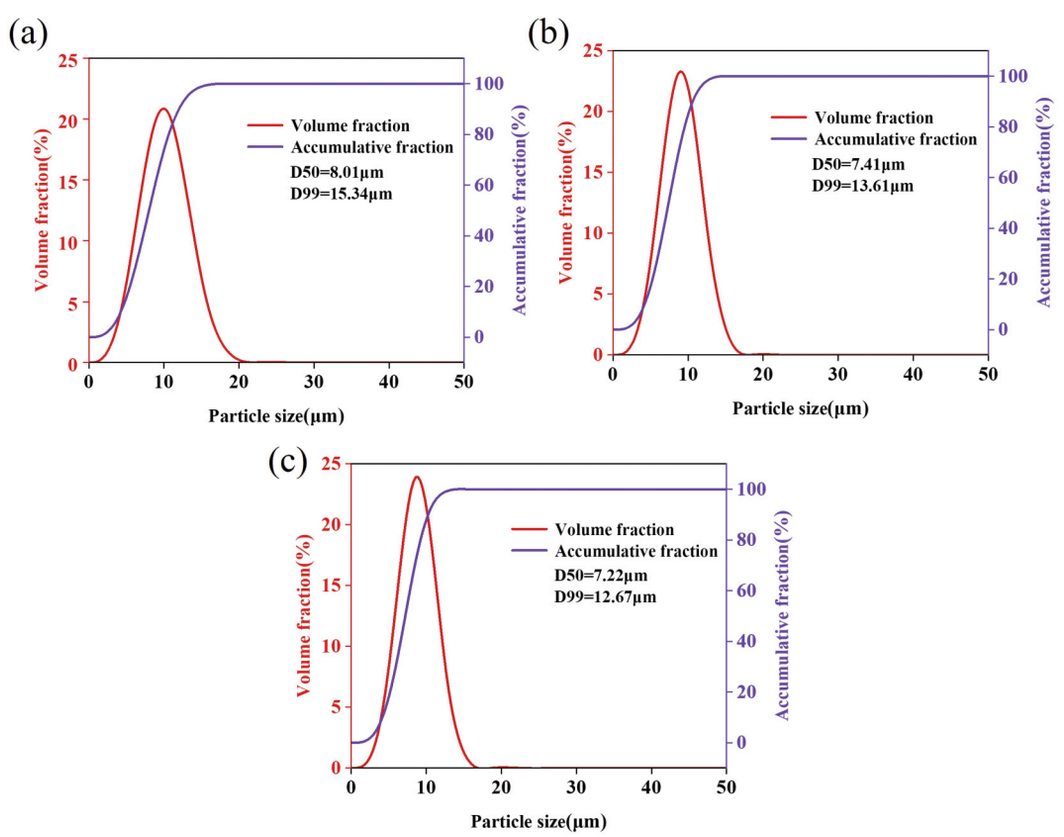

Figure 11. *Analysis results of iron phosphate particle size at different power: (a) 15W; (b) 35W; (c) 50W*

4. Conclusion

Ultrasonic acid leaching was used to remove impurities from iron phosphate under the following experimental conditions: Sulfuric acid concentration 0.2 mol·L^{-1}, acid-leaching time 30 min, power 50 W, and reaction temperature 80°C. Under these conditions, the removal rates of Cr, Cu, Ni, and Zn in the iron phosphate were 26.09%, 83.0%, 75.9%, and 96.3%, respectively. The iron phosphate was analyzed using XRD, TEM, XPS, and particle size characterization to elucidate the mechanism of impurity removal. The XRD diffraction pattern of the iron phosphate showed a sequential decrease in the intensity of the diffraction peaks with increasing power, with no other phases detected. Particle size analysis revealed that the iron phosphate particles were nearly spherical after ultrasonic leaching, indicating that the ultrasonic treatment changed the original shape of the iron phosphate during the impurity removal process. This study served as the basis for the introduction of other key technologies to achieve closed-loop recycling of lithium iron phosphate waste cathode materials, and solve the technical problems facing the development of the lithium battery recycling industry.

Acknowledgements

The authors wish to acknowledge the financial support on this research from the Talent Training Program of Yunnan of China (202005AC160041 and KKXY202252002).

Author's contributions

Conceptualization: Y. Zhao; methodology: Y. Zhao; software: Y.-H. Wang; validation: Y. Zhao and J.-J. Wu; formal analysis: Y. Zhao and J.-J. Wu; resources: J.-J. Wu and W.-H. Ma; writing—original draft preparation: Y. Zhao; writing—review and editing: Y. Zhao. All authors have read and agreed to the published version of the manuscript.

Data Availability Statement

The raw/processed data required to reproduce these findings cannot be shared at this time as the data also forms part of an ongoing study.

Conflict of interest statement

The authors declare that they have no known competing financial interests or personal relationships that could have appeared to influence the work reported in this paper.

References

[1] J.-H. Li, X.-L. Zeng, A. Stevels, Ecodesign in consumer electronics: past, present, and future, Critical Reviews in Environmental Science and Technology, 45 (2015) 840–860. https://doi.org/10.1080/10643389.2014.900245.

[2] J. Sencanski, D. Bajuk-Bogdanovic, D. Majstorovic, E. Tchernychova, J. Papan, M. Vujkovic, The synthesis of Li(Co-Mn-Ni)O_2 cathode material from spent-Li ion batteries and the proof of its functionality in aqueous lithium and sodium electrolytic solutions, Journal of Power Sources, 342 (2017) 690–703. https://doi.org/10.1016/j.jpowsour.2016.12.115.

[3] C.-W. Liu, J. Lin, H.-B. Cao, Y. Zhang, Z. Sun, Recycling of spent lithium-ion batteries in view of lithium recovery: A critical review, Journal of Cleaner Production, 228 (2019) 801–813. https://doi.org/10.1016/j.jclepro.2019.04.304.

[4] P. Byeon, H. Bin Bae, H.S. Chung, S.G. Lee, J.G. Kim, H.J. Lee, J.W. Choi, S.Y. Chung, Atomic-scale observation of $LiFePO_4$ and $LiCoO_2$ dissolution behavior in aqueous solutions, Advanced Functional Materials, 28 (2018) 1804564. https://doi.org/10.1002/adfm.201804564.

[5] J. Kumar, R.R. Neiber, J. Park, R.A. Soomro, G.W. Greene, S.A. Mazari, H.Y. Seo, J.H. Lee, M. Shon, D.W. Chang, K.Y. Cho, Recent progress in sustainable recycling of $LiFePO_4$-type lithium-ion batteries: Strategies for highly selective lithium recovery, Chemical Engineering Journal. 431 (2022) 133993. https://doi.org/10.1016/j.cej.2021.133993.

[6] S. Gu, L. Zhang, B.-T. Fu, X.-P. Wang, J.W. Ahn, Feasible route for the recovery of strategic metals from mixed lithium-ion batteries cathode materials by precipitation and carbonation, Chemical Engineering Journal, 420 (2020) 127561. https://doi.org/10.1016/j.cej.2020.127561.

[7] W.-B. Lou, Y. Zhang, Y. Zhang, S.-L. Zheng, P. Sun, X.-J. Wang, S. Qiao, J.-Z. Li, Y. Zhang, D.-Y. Liu, M. Wenzel, J.-J. Weigand, A facile way to regenerate $FePO_4{\cdot}2H_2O$ precursor from spent lithium iron phosphate cathode powder:spontaneous precipitation and phase transformation in an acidic medium, Journal of Alloys and Compounds, 856 (2020) 158148. https://doi.org/10.1016/j.jallcom.2020.158148.

[8] H. Mahandra, A. Ghahreman, A sustainable process for selective recovery of lithium as lithium phosphate from spent $LiFePO_4$ batteries, Resources Conservation and Recycling, 175 (2021) 105883. https://doi.org/10.1016/j.resconrec.2021.105883.

[9] P. Moazzam, Y. Boroumand, P. Rabiei, S.S. Baghbaderani, P. Mokarian, F. Mohagheghian, L.J. Mohammed, A. Razmjou, Lithium bioleaching: An emerging approach for the recovery of Li from spent lithium ion batteries, Chemosphere, 277 (2021) 130196. https://doi.org/10.1016/j.chemosphere.2021.130196.

[10] X.-H. Zheng, Z.-W. Zhu, X. Lin, Y. Zhang, Y. He, H.-B. Cao, Z. Sun, A mini-review on metal recycling from spent lithium ion batteries, Engineering, 4 (2018) 361–370. https://doi.org/10.1016/j.eng.2018.05.018.

[11] X.-P. Chen, B.-L. Fan, L.-P. Xu, T. Zhou, J.-R. Kong, An atom-economic process for the recovery of high value-added metals from spent lithium-ion batteries, Journal of Cleaner Production. 112 (2015) 3562–3570.

https://doi.org/10.1016/j.jclepro.2015.10.132.

[12] Y.-X. Yang, X.-H. Zheng, H.-B. Cao, C.-L. Zhao, X. Lin, P.-G. Ning, Y. Zhang, W. Jin, Z. Sun, A closed-loop process for selective metal recovery from spent lithium iron phosphate batteries through mechanochemical activation, ACS Sustainable Chemistry & Engineering, 5 (2017) 9972–9980. https://doi.org/10.1021/acssuschemeng.7b01914.

[13] W.-F. Gao, X.-H. Zhang, X.-H. Zheng, X. Lin, H.-B. Cao, Y. Zhi, Z. Sun, Lithium carbonate recovery from cathode scrap of spent lithium-ion battery– A closed-loop process, Environmental Science & Technology, 51 (2017) 1662–1669. https://doi.org/10.1021/acs.est.6b03320.

[14] D.-Y. Wu, D.-X. Wang, Z.-Q. Liu, S. Rao, K.-F. Zhang, Selective recovery of lithium from spent lithium iron phosphate batteries using oxidation pressure sulfuric acid leaching system, Transactions of Nonferrous Metals Society of China, 32 (2022) 2071–2079. https://doi.org/10.1016/S1003-6326(22)65931-4.

[15] S. Ghassa, A. Farzanegan, M. Gharabaghi, H. Abdollahi, Iron scrap, a sustainable reducing agent for waste lithium ions batteries leaching: An environmentally friendly method to treating waste with waste, Resources Conservation and Recycling, 166 (2021) 105348. https://doi.org/10.1016/j.resconrec.2020.105348.

[16] P.-C. Ning, Q. Meng, P. Dong, J.-G. Duan, M.-L. Xu, Y. Lin, Y.-J. Zhang, Recycling of cathode material from spent lithium ion batteries using an ultrasound-assisted DL-malic acid leaching system, Waste Management, 103 (2020) 52–60. https://doi.org/10.1016/j.wasman.2019.12.002.

[17] L.-Q. Zhuang, C.-H. Sun, T. Zhou, H. Li, A.-Q. Dai, Recovery of valuable metals from $LiNi_{0.5}Co_{0.2}Mn_{0.3}O_2$ cathode materials of spent Li-ion batteries using mild mixed acid as leachant, Waste Management, 85 (2019) 175–185. https://doi.org/10.1016/j.wasman.2018.12.034.

[18] L. Li, W.-J. Qu, X.-X. Zhang, J. Lu, R.-J. Chen, F. Wu, K. Amine, Succinic acid-based leaching system: A sustainable process for recovery of valuable metals from spent Li-ion batteries, Journal of Power Sources, 282 (2015) 544–551. https://doi.org/10.1016/j.jpowsour.2015.02.073.

[19] M. Esmaeili, S.O. Rastegar, R. Beigzadeh, T. Gu, Ultrasound-assisted leaching of spent lithium ion batteries by natural organic acids and H_2O_2, Chemosphere, 254 (2020) 126670. https://doi.org/10.1016/j.chemosphere.2020.126670.

[20] L.-M. Yang, Y.-F. Feng, C.-Q. Wang, D.-F. Fang, G.-P. Yi, Z. Gao, P.-H. Shao, C.-L. Liu, X.-B. Luo, S.-L. Luo, Closed-loop regeneration of battery-grade $FePO_4$ from lithium extraction slag of spent Li-ion batteries via phosphoric acid mixture selective leaching, Chemical Engineering Journal, 431 (2022) 133232. https://doi.org/10.1016/j.cej.2021.133232.

[21] M. Dular, O.C. Delgosha, M. Petkovšek, Observations of cavitation erosion pit formation, Ultrasonics Sonochemistry, 20 (2013) 1113–1120. https://doi.org/10.1016/j.ultsonch.2013.01.011.

[22] F. Jiang, Y.-Q. Chen, S.-H. Ju, Q.-Y. Zhu, L.-B. Zhang, J.-H. Peng, X.-M. Wang, J.D. Miller, Ultrasound-assisted leaching of cobalt and lithium from spent lithium-ion batteries, Ultrasonics Sonochemistry, 48 (2018) 88–95. https://doi.org/10.1016/j.ultsonch.2018.05.019.

[23] L. Castro, R. Dedryvère, M. El Khalifi, P.E. Lippens, J. Bréger, C. Tessier, D. Gonbeau, The spin-polarized electronic structure of $LiFePO_4$ and $FePO_4$ evidenced by in-lab XPS, Journal of Physical Chemistry C, 114 (2010) 17995–18000. https://doi.org/10.1021/jp106631v.

[24] Z. Li, D.-F Liu, J.-C. Xiong, L.-H. He, Z.-W. Zhao, D.-Z. Wang, Selective recovery of lithium and iron phosphate/carbon from spent lithium iron phosphate cathode material by anionic membrane slurry electrolysis, Waste Management, 107 (2020) 1–8. https://doi.org/10.1016/j.wasman.2020.03.017.

[25] X.-J. Wang, S.-L. Zheng, Y. Zhang, Y. Zhang, S. Qiao, Z.-Q. Long, B. Zhao, Z.-F. Li, Sulfuric acid leaching of ball-milling activated $FePO_4$ residue after lithium extraction from spent lithium iron phosphate cathode powder, Waste Management, 153 (2022) 31–40. https://doi.org/10.1016/j.wasman.2022.08.009.

ISPITIVANJE POSTUPKA UKLANJANJA NEČISTOĆA IZ ŠLJAKE KOJA SADRŽI FOSFATE LITIJUMA I GVOŽĐA POMOĆU ULTRASONIČNOG LUŽENJA SUMPORNOM KISELINOM

Y. Zhao [a], Y.-H. Wang [a], J.-J. Wu [a, b], W.-H. Ma [a, b]

[a] Fakultet za metalurško i energetsko inženjerstvo, Univerzitet za nauku i tehnologiju u Kuenmingu, Kuenming, Kina

[b] Državni inženjerski centar za istraživanje vakuumske metalurgije, Univerzitet za nauku i tehnologiju u Kuenmingu, Kuenming, Kina

Apstrakt

Dobijanje fosfata gvožđa iz šljake nastale prilikom postupka luženja katodnih materijala sa sadržajem fosfata gvožđa i litijuma predstavlja ključni korak za postizanje zatvorene petlje za dobijanje fosfata gvožđa i litijuma, što do sada nije postignuto. U ovom istraživanju je primenjeno ultrasonično luženje sumpornom kiselinom kako bi se uklonile nečistoće iz fosfata gvožđa kako bi se zadovoljili strogi zahtevi koji postoje za kvalitet baterija sa fosfatom gvožđa i sadržaj nečistoća. Optimizacija uslova luženja uključivala je koncentraciju sumporne kiseline od 0,2 mol·L^{-1}, vreme luženja od 30 minuta, snagu od 50 W i temperaturu reakcije od 80℃.

Pod ovim uslovima, efikasnost uklanjanja Cr, Cu, Ni i Zn iz fosfata gvožđa bile su 26,09%, 83,0%, 75,9% i 96,3%. Istovremeno, sadržaj nečistoće Cr i Zn bio je u skladu sa standardom za kvalitet baterije koja sadrži fosfat gvožđa (HG/T 4701-2021), i to na nivou od 50 ppm i 10 ppm. Rezultati luženja pokazali su da je ultrazvuk efikasan u uklanjanju nečistoća iz fosfata gvožđa u rastvoru sumporne kiseline. Dalja analiza, uključujući XRD, veličinu čestica, TEM i XPS, pokazala je da je na površini čestica fosfata gvožđa došlo do kavitacije nakon ultrazvučnog luženja kiselinom, što je dovelo do formiranja brojnih pora. Pored toga, sudari čestica doveli su do smanjenja veličine čestica bez formiranja nusproizvoda tokom procesa. Ovaj inovativni pristup ne samo da je doprineo uklanjanju elemenata nečistoće, već je pružio i uvid u ponovnu upotrebu šljake nastale prilikom luženja (fosfat gvožđa) i ponudio smernice za dobijanje metala iz otpadnih katodnih materijala sa sadržajem litijuma i gvožđa.

Ključne reči: *Fosfat gvožđa; Ultrasonično luženje kiselinom; Kvalitet baterije; Ponovna upotreba*